

PAPER • OPEN ACCESS

Intentional and unintentional channeling during implantation of ^{51}V ions into 4H-SiC

To cite this article: M K Linnarsson *et al* 2019 *Semicond. Sci. Technol.* **34** 115006

View the [article online](#) for updates and enhancements.



IOP | ebooksTM

Bringing together innovative digital publishing with leading authors from the global scientific community.

Start exploring the collection—download the first chapter of every title for free.

Intentional and unintentional channeling during implantation of ^{51}V ions into 4H-SiC

M K Linnarsson^{1,4} , A Hallén²  and L Vines³ 

¹ Materials and Nano-Physics, Department of Applied Physics, School of SCI, KTH Royal Institute of Technology, Electrum 229, SE-164 40 Kista, Sweden

² School of EECS, KTH Royal Institute of Technology, Electrum 229, SE-164 40 Kista, Sweden

³ Physics Department/Center for Materials Science and Nanotechnology, University of Oslo, PO Box 1048 Blindern, N-0316 Oslo, Norway

E-mail: marga@kth.se, ahallen@kth.se and lasse.vines@fys.uio.no

Received 25 June 2019, revised 23 August 2019

Accepted for publication 4 September 2019

Published 1 October 2019



CrossMark

Abstract

Ion implantation is a commonly used process step in 4H-SiC device manufacturing to implement precise concentrations of dopant atoms in selected areas and depths. This paper reports on vanadium (V) implantation into 4H-SiC(0001) and how the crystal lattice, with preferential directions, channels, for the ions, will influence the final dopant distribution. Concentration versus depth profiles of V-ions, intentionally and unintentionally channelled, has been recorded by secondary ion mass spectrometry. Ion implantations have been performed between 50 and 300 keV at various impact angles and fluence at room temperature as well as at elevated temperatures. Before ion implantation, the samples were aligned utilizing the blocking pattern of 100 keV backscattered protons. In addition to the aligned implantations, our standard beam line for ion implantation has been used for implantations in a ‘random’ direction using the wafer miscut angle of 4° . The electronic stopping has been determined from these ‘random’ cases and the values have been used in 3D simulations to predict preferential crystallographic directions using SIIMPL, a Monte Carlo simulation code based on the binary collision approximation. The results show that, independent of the used impact angle there is always a probability that the vanadium ions will be steered into the [000-1] and the family of $\langle 11-2-3 \rangle$ crystal directions and therefore penetrate deep into the sample, resulting in unwanted ‘spikes’. If the implantation is performed at elevated temperatures, a larger degree of dechanneling is present due to increased thermal vibrations and the penetration depth of vanadium is slightly reduced.

Keywords: aligned ion implantation, Monte-Carlo simulation, electronic stopping, binar collision approximation, SIMS

(Some figures may appear in colour only in the online journal)

1. Introduction

Ion implantation is today a well-established technique for introduction of dopants into 4H-SiC since, (i) diffusion of

dopants is not applicable due to low diffusivity and (ii) epitaxial growth may not be a useful alternative, particularly for locally confined volumes. Vanadium offers several deep levels in 4H-SiC for charge trapping and recombination and is used as one alternative for semi insulating substrates and may be employed to electrically isolate local areas on devices, or for local life-time control [1–3]. Here ion implantations offer an excellent alternative to control vanadium 3D dopant distribution.

After room temperature (RT) implantations in SiC a high temperature post implant annealing step is needed for full activation of dopants and healing of the lattice damage. The

⁴ Author to whom any correspondence should be addressed.



Original content from this work may be used under the terms of the [Creative Commons Attribution 3.0 licence](https://creativecommons.org/licenses/by/3.0/). Any further distribution of this work must maintain attribution to the author(s) and the title of the work, journal citation and DOI.

need for this demanding process can partly be eased by using hot implants to reduce the implantation induced damage and preserve the crystalline properties during particularly high fluence implantations. However, the crystalline structure of the sample during implantation is also affecting the obtained depth distribution. In fact, the so called channeling may considerably increase the ion penetration depth in crystalline material compared to an amorphous target. This phenomenon may occur if the direction of the incident ion beam is nearly in parallel to major crystallographic axes or planes. In these directions, the reduction of energy loss per path length for the ion is less and therefore ions move deeper into the target.

Channeling is most often an unwanted effect, and, typically, the SiC wafer is oriented in some random, non-channeling, direction to minimize channeling effects during implantation. For example, as implantation direction in 4H-SiC (hexagonal silicon carbide), a 4° off-axis from the [0001] towards the [11-20] direction is often used as a 'random' direction, taking advantage of the standard miscut angle of SiC wafers. This results in more or less Gaussian shaped dopant versus depth profiles, where the depth is determined by the energy, the used ions and the target atoms. Nevertheless a few ions usually find a crystal channel [4–7], which results in a protrusions of the dopant distribution extending considerably deeper than expected for non-channeled ions and may be influencing, for instance, the position of an electrical pn-junction. On the other hand, if the implantation is performed along a crystallographic axis a completely different profile will be obtained where the ions follow the crystal direction deep into the target [7, 8]. In SiC, it has been shown that the deepest channeled ions may penetrate many times the projected range of the corresponding random implant [9–11], and recently attempts to utilize these effects in SiC devices has even been reported [12, 13]. However, implantation is usually performed at elevated temperatures to avoid damage [14, 15]. For such implantations, thermal vibrations will increase and therefore channeling may decrease [11]. Channeling is also altered by the presence of a surface top-layer consisting of adhesive contaminants and natural or intentionally added oxides [16]. To complicate the situation further, the lattice damage caused by the ions is reduced for elevated temperature implants due to dynamic annealing, but the damage may also be reduced for channeling implantations [17–19].

To theoretically describe the probability for channeling, the concept of 'critical angle for channeling' was introduced by Lindhard in the 1960s [20, 21]. Here, the critical angle is taken as the maximum angle between the axial rows of atoms and the incoming beam for which the ions still will be steered along the axis. The usefulness of this prediction has been experimentally verified in many semiconductors [22]. To further investigate and predict channeling phenomena during ion implantation, nowadays several codes for Monte Carlo simulation in crystalline targets exists, using the binary collision approximation (MC-BCA) [23–27]. In this context, it should be mentioned that most BCA codes of today stem from the algorithms described by Robinson *et al* in the 1960s that was implemented in the so-called MARLOWE code

[28, 29]. Furthermore, modifications of the electronic stopping in channels are usually included as a modified version of the concept introduced by Oen *et al* [30] and thermal vibration are typically treated according to Barrett-based approach [31].

In this study, we have investigated intentional and unintentional channeling during ion implantation of ^{51}V into 4H-SiC. Wafers with the standard 4H-SiC geometry, (0001) with an off-axis miscut of about 4° towards $\langle 11-20 \rangle$ direction, have been used. Before implantation, the crystal has been aligned and angles of incidence between 0° and 17° have been investigated. Both RT and elevated temperatures have been employed. To support experimental results, Monte-Carlo simulations have been performed utilizing the binary collision approximation (MC-BCA) code SIIMPL [27]. Experimental data in combination with simulations show that a fully non-channeling direction is hard to find and independent of the used impinging ion direction, a certain amount of ions will be steered, particularly into [0001] and $\langle 11-23 \rangle$ channels and travel to substantial depth.

2. Experimental

Samples with a size of $5 \times 11 \text{ mm}^2$ have been cut from a 4H-SiC wafer with an n-type ($5 \times 10^{15} \text{ N cm}^{-3}$), $10 \mu\text{m}$ thick, epitaxial layer. Before implantation, the sample was aligned and the crystal orientation relative to the incoming beam was determined. For the sample alignment, 100 keV protons were employed and a 6-axis, high-precision, goniometer was used. The blocking pattern for the backscattered protons was recorded with an area sensitive, 120 mm, diameter detector. After alignment, the ion source is reconfigured to produce $^{51}\text{V}^+$ -ions and ion implantation was subsequently performed with $^{51}\text{V}^+$ ions with energies between 50 and 200 keV at a fluence between 8.7×10^{11} and $1.9 \times 10^{14} \text{ cm}^{-2}$ in $1.5 \times 1.5 \text{ mm}^2$ regions at different positions on the same sample surface. No scanning of the beam has been done for this implantation and the implanted areas have been determined by three pairs of *x*- and *y* slits in the 10 m long beam line. Impact angles with tilt from 0° , i.e., [0001] to 17° towards the $\langle 11-20 \rangle$ direction, as well as RT and elevated temperatures have been used. Implantations started at RT, followed by implantations at 500°C and subsequent, implantations at 300°C and 150°C in different areas of the same sample. For each temperature, different fluence have been used, where 'low' fluence should be low enough to have negligible contribution to de-channeling from built-up damage and 'high' fluence should be high enough for the channeling phenomena to saturate due to channels being blocked by interstitials. The beam current is kept constant and different fluence is accumulated during implantation times from a few seconds to 10–15 min. Typically, a current density of 0.5 nA mm^{-2} was employed and the samples were placed on a molybdenum plate to give high thermal conductivity and avoid heating by the ion beam. In addition, five implantations of ^{51}V at energies between 50 and 300 keV were performed in our standard set up for ion implantation utilizing the miscut of

4° of the wafer. These fluence were determined by current integration.

The vanadium depth distribution in the 4H-SiC samples were determined by secondary ion mass spectrometry (SIMS) using a Cameca ims7f instrument. A primary sputtering beam of 10 keV $^{32}\text{O}_2^+$ ions was applied and secondary $^{51}\text{V}^+$ ions were detected. The primary beam was typical rastered over an area of $200 \times 200 \mu\text{m}^2$ and the ion signal was recorded from the central part of this area (diameter $\sim \Phi 60 \mu\text{m}$). Calibration of the V signal is performed using an implanted reference sample. This implantation has been made in 4H-SiC at RT using 180 keV ^{51}V -ions to a dose of $1 \times 10^{13} \text{cm}^{-2}$. Crater depths were measured with a Dektak 8 stylus profilometer and a constant erosion rate was assumed for the conversion from sputter time versus depth. The fluence was precisely determined by integration of the concentration versus depth profiles.

3. Simulations

To predict and compare experimental recorded depth profiles, simulations were performed using the Monte-Carlo binary collision approximation (MC-BCA) code SIIMPL [27]. The universal potential of Ziegler, Biersack and Littmark [32] is used and the scattering integral is solved by the ‘Magic-Formula’ [33]. This program also accounts for the build-up of damage as a function of fluence. Both the Kinching Pease [34] and a full cascade model have been used to estimated number of displaced atoms and the increasing annealing of damages at elevated temperatures has been accounted for. The probability that the next collision will be a collision with an implantation induced interstitial scales with the local density of damage. This probability increases as the fluence increases and more damage is accumulated. A fitting parameter, c_a , accounts for the defect kinetics occurring after the ballistic phase of the damage formation and includes recombination of point defects during the implantation, so called dynamic annealing, and the probability for formation of stable defects. These effects are typically strongly temperature dependent which is included in c_a . For instant the c_a factor is twice as high at RT compared to 500 °C for implantations in 4H-SiC [10, 27]. The electronic stopping, S_e , for the used energies ($E < E_F$, E_F is related to the Fermi velocity of the target valence electrons, which in SiC translates to about $E_F/M_1 = 35 \text{keV amu}^{-1}$ with $M_1 = 51 \text{amu}$ for vanadium) is expressed as [35]

$$S_e = kE^b, \quad (1)$$

where the constants k and b are determined from experimental data for ‘random’/non-channeled implantations. In order to describe the lower electronic stopping in channels, the random electronic loss, S_e , has been modified and is given by

$$\Delta E = S_e A \exp(-sp/a_u), \quad (2)$$

where A , p and a_u are a normalization constant, the impact parameter and the universal screening length, respectively [26]. The parameter s is treated as a fitting parameter where the intention is to tune the interaction between ions and lattice

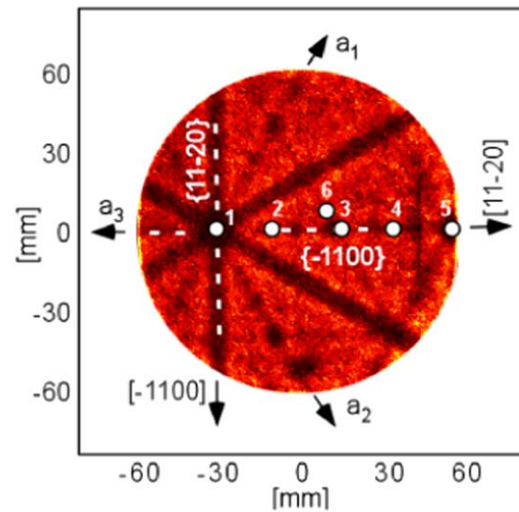


Figure 1. Blocking pattern from backscattered 100 keV protons on 4H-SiC, where darker areas represent lower intensity. The detector covers an angle of 22°. A few planes and directions are indicated. Number 1–6 show the direction used for the implants. 1: [0001], 2: 4° off from [0001] towards [11-23], 3: 9° off, 4: 13° off, 5: 17° off = [11-23], and 6: rotated 8° around the [-1100] direction followed by a rotation of 11° around the [0001] direction.

atoms by an exponentially declining potential and modify the screening length to improve the description of the interaction between the target atoms and the ions in the channels. As the range of channelled ions depends on dechanneling probability as well as on the inelastic energy loss, which may differ between channels, s may not necessary have the same value for different channels. In this contribution literature values for the mean vibration amplitude at RT have been utilized in the simulations [36]. At elevated temperatures, the mean vibration amplitude has been treated as a fitting parameter in agreement with our previous result for Al channeling in 4H-SiC [37]. Furthermore, the non-aligned, sample top-layer (including the self-oxide) is represented by an amorphous SiC layer in the simulations. An 8 Å thick layer has been used for simulations at RT while a 4 Å thick, amorphous SiC top-layer have been assumed at elevated temperatures. The RT thickness is according to literature [38] where a 9 Å thick native oxide, a silicon oxycarbide, is expected after exposure of SiC to air, as measured by angle-resolved x-ray reflectivity. The small difference between 8 and 9 Å is due to a slightly lower density of the silicon oxycarbide layer compared to amorphous SiC utilized in the simulation. The reduction of the top-layer to 4 Å at elevated temperatures is based on simulations and is motivated by possible desorption of surface contaminants as well as improvement of the lattice match of the self-oxide.

4. Results

4.1. Crystal structure and beam alignment

Blocking patterns can be used to find channeling direction, as channeling and blocking patterns are equivalent according to rules of reversibility. In figure 1(a) blocking pattern/backscattering

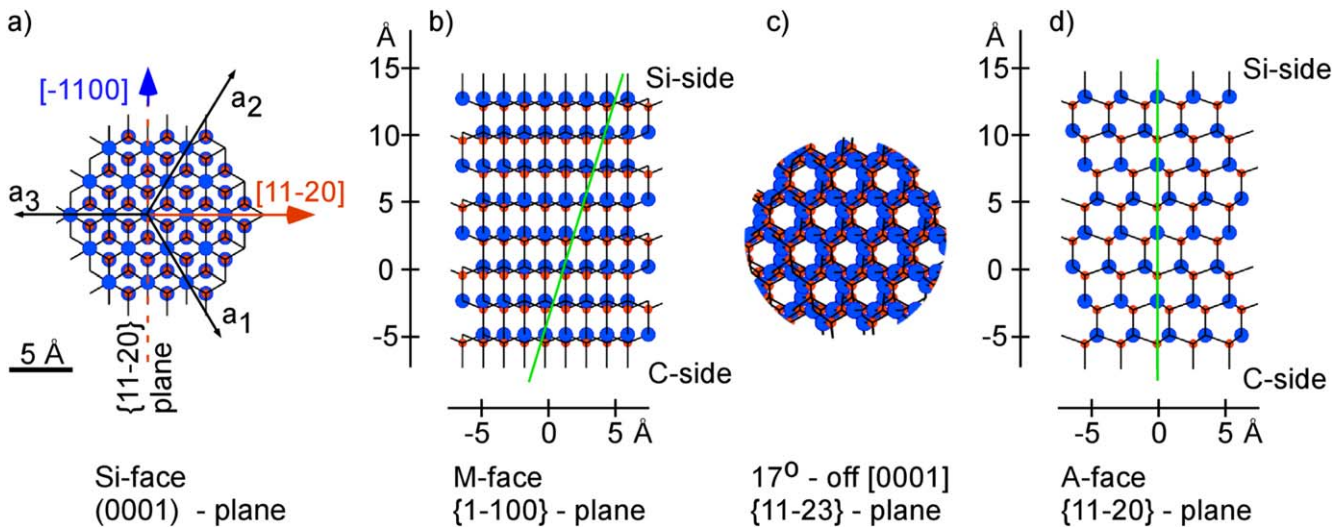


Figure 2. (a)–(d) Sketch of atomic positions at four crystal planes in 4H-SiC. Blue and red dots represent silicon and carbon atoms, respectively. The Si-face (a), the M-face (b), a 17° -off plane, i.e. a $\{11-23\}$ plane (c) and A-face (d) are shown. In (a) arrows indicate the direction of lattice vectors as well as the $[-1100]$ and the $[11-20]$ directions. The plane $\{11-20\}$ is indicated by a red dashed line in (a). In (b) and (d), the full green line shows a tilt angle 17° from $[000-1]$ in the $\{1-100\}$ plane, towards the $[11-20]$ direction. The lattice parameters are: $c = 10.52 \text{ \AA}$ and $a = 3.073 \text{ \AA}$ where $|(11-20)| = 3|a|$.

image is shown for 4H-SiC recorded with 100 keV protons. Darker areas represent lower intensity and shows the position of axial and planar channels. In total, an angle of 22° is covered by the detector. The detector, is mobile and both the sample and the detector are rotated relative to the incoming beam to record both the blocking pattern in the $[0001]$ direction and the $\langle 11-23 \rangle$ direction, 17° apart in the $\{1-100\}$ plane. The six-fold symmetry is seen from $\{11-20\}$ and $\{1-100\}$ planes crossing at the $[0001]$ direction. These kind of blocking patterns was used to align the sample before performing the $^{51}\text{V}^+$ implantation along a well-defined direction. Furthermore, the used implantation directions have been indicated in figure 1 with numbered white dots.

However, the critical angle for channeling of $^{51}\text{V}^+$ -ions differ from $^1\text{H}^+$ -ions because the ‘width’ of channels increases with decreasing energy and increasing atomic numbers [7]. For example, a larger critical angle is expected for $^{51}\text{V}^+$ -ions compared to $^1\text{H}^+$ -ions of the same energy, while increasing the $^{51}\text{V}^+$ energy from 100 and 200 keV, a 20% reduction of the critical angle for channeling due to the $E^{-1/4}$ dependence is expected. Furthermore, for more narrow channels the width is strongly reduced by lattice vibrations and imperfections in the crystal [7, 11, 31].

To facilitate identification of the used geometries, the atomic positions are sketched in figures 2(a)–(d) at four different 4H-SiC planes. Blue dots represent silicon atoms and red dots carbon atoms. Black lines are used to indicate bonds between carbon and silicon atoms. In figure 2(a), the Si-face (0001) plane is shown and the direction of the hexagonal lattice vectors a_1 , a_2 and a_3 are indicated. The hexagonal lattice vector $[0001]$ is perpendicular to the plane of the paper. Furthermore, the family members of the $\langle 11-20 \rangle$ and the $\langle -1100 \rangle$ directions, as well as position of one $\{11-20\}$ plane, the so called A-face (figure 2(d)), are indicated in figure 2(a). The $\{1-100\}$ plane, the so-called M-face (figure 2(b)), is perpendicular to the A-face. The projection of $\langle 11-23 \rangle$

direction, the 17° off angle, has been included in figures 2(b) and (d) as a green line.

Turning the sample in the $\{1-100\}$ plane from the $[0001]$ direction towards a $\langle 11-23 \rangle$, 17° off from $[0001]$, a widely open direction is reached, as shown in figure 2(c). In this family of crystal directions, implanted ions can relatively easy find their way into the channels, even though samples are deliberately misaligned to avoid channeling, as discussed under paragraph 4.2 and 4.3.

4.2. Electronic stopping and ‘random’ implantation directions

For practical reasons, implantation into 4H-SiC, a 4° off-axis from the $[0001]$ towards the $[11-20]$ direction is often employed as a non-channeling direction, taking advantage of the standard miscut of wafers. However, this may not be the best choice to avoid channeling along $[000-1]$ as a critical angle between 3° and 4° is expected at RT for 100 keV vanadium ions [5, 20, 21].

In this study, this geometry has been used to determine values for electronic stopping for later use in simulations. Figure 3(a) shows experimental data for ^{51}V implantations performed between 50 and 300 keV at RT with fluence between 1.7×10^{12} and $1.9 \times 10^{12} \text{ cm}^{-2}$. The used fluence are below the point where damage contributes significantly to dechanneling. It is clearly seen from the curve shape in figure 3(a), that a few ions have found an open crystal direction resulting in an extended distribution at a concentration of around one percent of the peak concentration, displaying an abrupt stop and reaching much deeper into the sample than expected for an amorphous target. The curves have a pronounced knee and as the energy increases, the concentration at the kink decreases. This decrease is most likely related to decreasing critical angles for increasing energies and therefore less ions will follow the $[000-1]$ direction. As the energy

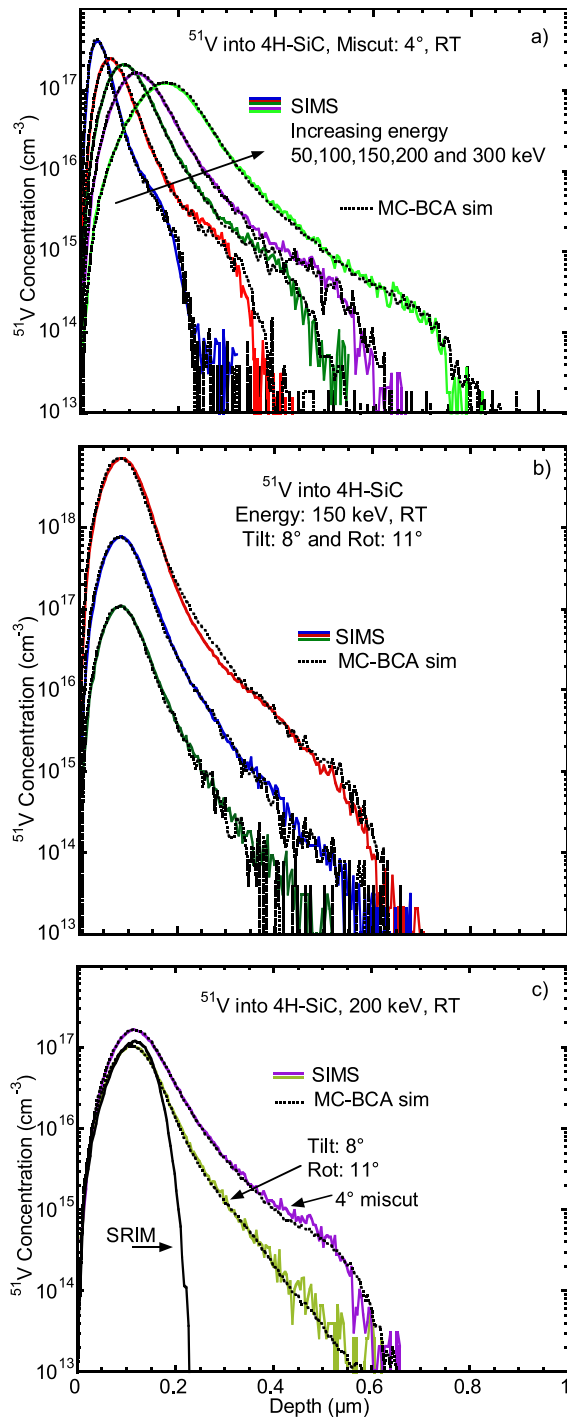


Figure 3. Depth distribution measured by SIMS of ^{51}V implanted into 4H-SiC at RT. MC-BCA simulation results obtained with the SIIMPL code have been included as black dotted lines. In (a), five samples have been implanted with 50, 100, 150, 200 or 300 keV and fluence $(1.7\text{--}1.9) \times 10^{14}\ \text{cm}^{-2}$ at an impact angle of 4° , using the miscut angle of the wafer. (b) Displays three implantations at 150 keV and fluence of 8.7×10^{11} , 6.2×10^{12} and $5.8 \times 10^{13}\ \text{cm}^{-2}$ performed in a ‘random’ direction here represented by an 8° tilt in combination with rotation of 11° . In (c), results for the two directions used in (a) and (b) are compared for 200 keV ions and fluence of 1.8×10^{12} and $1.0 \times 10^{12}\ \text{cm}^{-2}$, respectively. In addition, the random depth profile from the SRIM code has been included in (c).

increases from 50 to 300 keV the critical angle for axial channeling in [0001] direction decreases from 4° to 3° at RT. MC-BCA simulations have been performed to fit the experimental results and are included as black dotted lines in figure 3(a). These simulations have been used to determine the constants k and b in equation (1) and a random electronic stopping, $S_e = 6.0E^{0.45}\ \text{eV}/(10^{15}\ \text{atoms}\ \text{cm}^{-2})$, where E is given in keV, has been determined. If the constants k and b are extracted in the used range from the SRIM package 2013, a stopping power of $5.8E^{0.5}$ is obtained [39]. The agreement is quite good where slightly higher stopping is suggested by SRIM. This may be due to the very limited energy range used in this investigation, or a lack of accurate experimental data in the SRIM data base. According to the blocking pattern in figure 1, it may be possible to find a direction with less unintentional channeling. For this reason, the sample has been rotated 8° around the $[-1100]$ direction followed by a rotation of 11° around the [0001] direction as an alternative to further reduce channeling, as shown in figure 3(b) for 150 keV $^{51}\text{V}^+$ -ions implanted at RT. Three different fluence, 8.7×10^{11} , 6.2×10^{12} and $5.8 \times 10^{13}\ \text{cm}^{-2}$ have been used. At 8.7×10^{11} , $6.2 \times 10^{12}\ \text{cm}^{-2}$, the measured depth profiles are smooth and have no pronounced kink around $0.25\ \mu\text{m}$, in contrast to the highest used fluence $5.8 \times 10^{13}\ \text{cm}^{-2}$. For the highest fluence, the implanted distribution is raised between 0.4 and $0.6\ \mu\text{m}$, and the ^{51}V concentration profile starts to resemble a channeled implantation. This effect may be explained by an increasing degree of damage close to the surface as the fluence increases. Hence, the probability for an ion to be scattered in any direction increases and therefore an increased number of ions may be within the critical angle for channeling [40]. Similar results, where the probability for channeling increases as the fluence increases, are also observed for implantations done at 50, 100 and 200 keV (not shown).

In figure 3(c), the measured depth distribution of 200 keV ^{51}V -ions is compared for two implantation directions, a tilt of 4° , and a combination of a tilt angle of 8° with a rotation of 11° . A slightly higher fluence was obtained for the sample with just 4° tilt. In addition to experimental data, MC-BCA simulations as well as SRIM calculations, with the same fluence as the sample with 8° tilt and 11° rotated sample, have been included and there is a clear difference between experimental data and SRIM results. Up to, and around the projected range, the distributions are similar, but the experimental depth distributions extends significantly deeper than the SRIM results. It is obvious that the influence from the crystal structure is pronounced and has to be considered in experimental work. At low fluence, channeling effects contribute less to the depth profile for the rotation of 11° plus tilt 8° sample (figure 3(b)). However, as the fluence increases, the portion of channeled ions increases. This means that in most applications it is no obvious gain to change implantation direction away from the standard 4° off angle as a non-channeling direction.

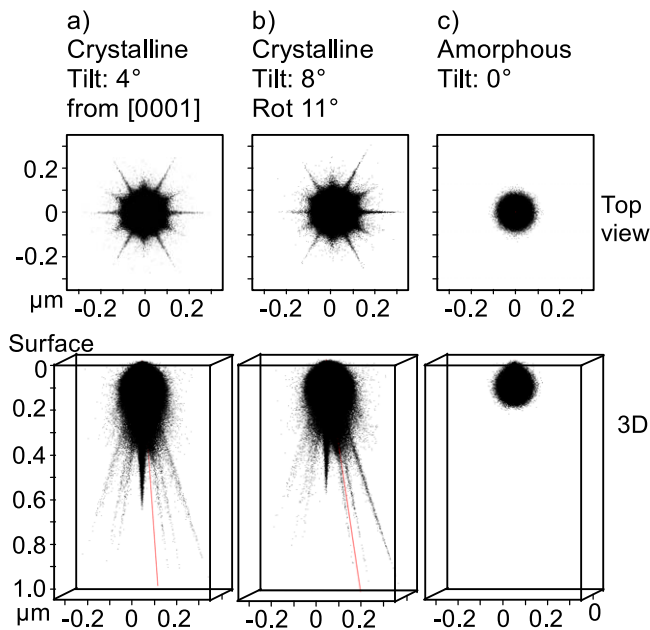


Figure 4. 3D simulations displaying the probability to find an implanted ion at a certain position in a 4H-SiC lattice after ion implantation. The MC-BCA code SIIMPL has been used in the simulations [27]. 200 keV $^{51}\text{V}^{+}$ -ions and an impact area of $1 \times 1 \text{ nm}^2$ has been employed. In (a) and (b) the crystal structure of 4H-SiC is used while in (c), an amorphous SiC target is employed with simulation parameters according to SRIM. Different angles for the incidence beam has been utilized, (a) 4° off from the [000-1] towards the $\langle 11-20 \rangle$ direction, (b) tilted 8° away from the [000-1] in addition to an 11° rotation from the $\{-1100\}$ plane and (c) along surface normal.

Three dimensional (3D) MC-BCA simulations, as shown in figure 4, have been performed to investigate the origin of the extended ‘tails’ in figure 3(c) and assign preferred crystallographic directions that contribute to this kind of profiles in 4H-SiC. In figures 4(a)–(c), the probability to find an implanted $^{51}\text{V}^{+}$ -ion at a particular position in the crystal is displayed. The used direction of the incoming beam is according to data in figure 3(c). Both the 3D images and top-views (XY-view) are included. The small black dots represent simulated ions and a higher density of dots means larger probability to find an ion. In the simulation 200 keV ions have been implanted within a rectangular area of $1 \times 1 \text{ nm}^2$. Please note that, using such small impact area, the fluence of dopants used in all device implantations always results in less than one ion and the 3D-simulations in figure 4 only displays probabilities to find an ion at a particular position.

In figure 4(a), the simulation is performed with the incoming beam entering from the top, perpendicular to the sample surface using the 4° miscut from the [000-1] direction towards the $\langle 11-20 \rangle$ direction. The 3D-image consists of a large 3D-scattered volume with a dark cone extended along the [000-1] direction down to about $0.6 \mu\text{m}$, meaning that there is a considerable probability for ^{51}V -ions to be scattered into the [000-1] direction. The extension in depth of the cone, as well as the intensity, indicates that the tails in figure 3(a) are mainly related to ions that are channeled in the [000-1] direction. According to the experimental data, 1D-depth

profiles for 4° miscut angle in figures 3(a) and (c), this protrusion between 0.4 and $0.6 \mu\text{m}$ is expected to be about 1% of the total ^{51}V content. Furthermore, the contribution from channeling of ^{51}V -ions along the family of $\langle 11-2-3 \rangle$ directions may not be negligible. These directions are clearly visible in the 3D-simulation as six, long ‘spikes’, laying on the surface of a cone, 17° from the [0001] direction. Although ions may travel deeper into the sample along $\langle 11-2-3 \rangle$ directions, the concentration is much lower and barely in the range for the detection limit of the SIMS measurements in figure 3(a). The top-view in figure 4(a) visualizes the six-fold symmetry with an increased contribution along the family of $\langle 11-2-3 \rangle$ directions, but an increased probability can also be seen in the $\{11-20\}$ planes.

Figure 4(b) shows the 3D ion distribution when the sample has been tilted 8° away from the [000-1] and rotated 11° from the $\{-1100\}$ plane. A red line in the figure indicates the implantation direction. No enhancement of ions along the red line is revealed, but instead the ions follow preferential crystal directions. The top-view shows the 6-fold symmetry and an increased probability for ion channeling along a $\langle 11-2-3 \rangle$ direction, but also an increased probability is seen along the $\{11-20\}$ planes 30° off from the $\{1-100\}$ planes. According to figure 4(b), the probability is slightly lower for ions to be scattered into the [000-1] direction compared to implantation at the 4° off (figure 4(a)). On the other hand, the probability increases for ions to be scattered into a $\langle 11-23 \rangle$ direction using an 8° tilt and a 11° rotation (figure 4(b)).

For an amorphous target, as assumed in SRIM calculations, only a drop-like distribution is expected (figure 4(c)). This shape means that ions are scattered roughly isotropically in depth as well as laterally. Starting at the surface with an impact area of 1 nm^2 , at the depth of $0.1 \mu\text{m}$ the lateral spread of ions is much larger and the probability to find an ion $0.1 \mu\text{m}$ lateral from the original direction is high. As expected, according to SRIM simulations, figure 4(c), do not include deep channeling tails and highlights the importance of including the crystal structure to properly describe experimental implantation profiles.

4.3. Aligned implantation directions

To further investigate the unintentional scattering into crystal channels, implantations have been performed along five different directions, starting at the [000-1] and rotating the sample in the $\{-1100\}$ plane towards the $\langle 11-20 \rangle$ direction. SIMS measurements are shown in figure 5 for 100 keV ^{51}V ions implanted at RT with 0° , 4° , 9° , 13° and 17° tilt away from [000-1]. Fluence in the range $(0.9-1.5) \times 10^{14} \text{ cm}^{-2}$ have been used.

At 0° , i.e. the [000-1] direction, the main peak is markedly broader ($0-0.2 \mu\text{m}$) and the maximum is at a larger depth compared to a random implantation ($0.06 \mu\text{m}$). In addition, a broad plateau ($0.2-0.4 \mu\text{m}$) is also observed caused by channeling in the [000-1] direction. Furthermore, an additional extension of the distribution is revealed between 0.4 and $0.5 \mu\text{m}$, that most likely originate from ions that have been scattered into a $\langle 11-2-3 \rangle$ direction. As the sample is

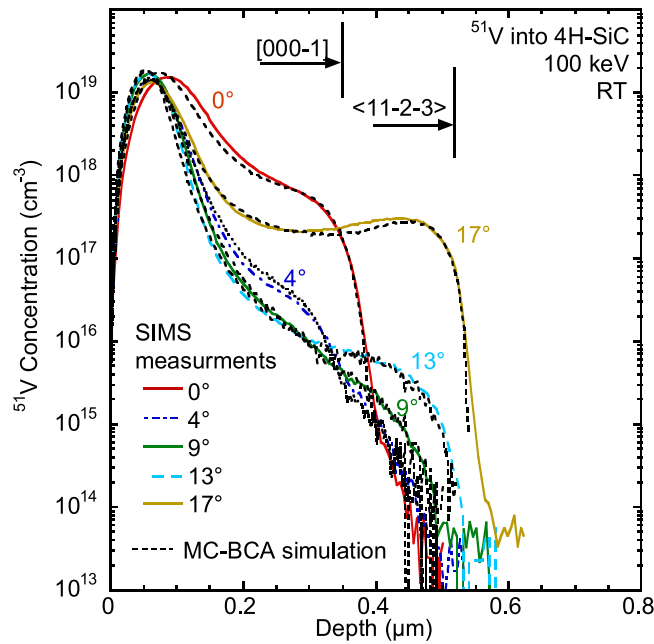


Figure 5. SIMS measurements and MC-BCA simulation with the code SIIMPL of five vanadium implantations into 4H-SiC. 100 keV $^{51}\text{V}^+$ -ions and fluence $(0.93\text{--}1.5) \times 10^{14} \text{ cm}^{-2}$ have been used. The ions are entering along the [000-1] direction, 0° off and towards [11-20] at 4° , 9° , 13° , 17° off angles where 17° corresponds to the [11-2-3] direction.

tilted away from [000-1], the concentration maximum has moved towards the surface and approach the position for a random implant. At 4° off from the [000-1], fewer ions are channelled into the [000-1] direction and the concentration decreases in the $0.2\text{--}0.4 \mu\text{m}$ range, while a small contribution from channeling in the $\langle 11-2-3 \rangle$ remains deeper than $0.35 \mu\text{m}$. At 9° , the contribution from [000-1] is further decreased while the contribution from the $\langle 11-2-3 \rangle$ direction increases. The probability for channeling into a $\langle 11-2-3 \rangle$ direction increases even more at 13° and reaches its maximum for an impact angle of 17° .

Simulations in 3D have been used to further support and substantiate the suggested preferential directions of impinging ions according to the experimental results in figure 5. Hence, in the simulations the angle of the impinging ions has been varied from [0001] towards the $\langle 11-20 \rangle$ direction, using angles off 0° (a), 4° (b), 9° (c), 13° (d) and 17° (e). An impact area of $1 \times 1 \text{ nm}^2$ has been used in the simulations to visualize preferred crystal directions and 5×10^6 ion tracks have been recorded. The simulation results are presented in figure 6 as 2D-images, extracted from the 3D-simulations. Both top views, (0001), and cross sections taken in the $\{-1100\}$ plane are shown. The top views include all ions used in the simulation as black dots. The position of the used cross section is indicated by a dashed red line in (a) and the direction of the corresponding beam as a dashed red line in cross sections below. For the cross sections, a linear concentration scale, is used and the same colour coding has been used for all figures. To exclude all scattering directions not laying in the $\{-1100\}$ plane, only a 1 nm thick slice is displayed. This is done to simplify identification of channel

directions in this plane, not being confused by the 6-fold symmetry. The fluence $1 \times 10^{14} \text{ cm}^{-2}$ is used in the simulations to also include scattering due to build-up of damage, which is in agreement with the experimental data in figure 5.

In figure 6(a), with the beam entering along the [000-1] direction, the main part of ions will follow the [000-1] direction but a minor contribution, a very weak signal, is coming from de-channelled ions that have been scattered into $\langle 11-23 \rangle$ directions at 17° off from the [000-1] direction. The contribution from these ions, along [11-2-3] and [-1-1 2-3] directions, are extending deeper into the crystal compared to ions that follows the [000-1] direction fully in agreement with experimental data in figure 5, where extended tails between 0.4 and $0.5 \mu\text{m}$ are recorded. At 4° off, figure 6(b), the contribution from the [000-1] direction decreases, as expected from the experimental SIMS data (figure 5), and the probability for an ion to be scattered into the $\langle 11-2-3 \rangle$ family increases. Turning the sample to 9° off angle, a further decrease of the contribution from [000-1] is observed, while the probability for an ion to be channelled into the [11-2-3] direction is increased. At this angle, the probability for ions to be channelled into different $\langle 11-2-3 \rangle$ directions start to differ and the probability for [-1-1 2-3] decreases, while the probability for entering [11-2-3] increases. This separation is even more pronounced at 13° off, shown in figure 6(d). In addition, in the 13° off sample, a new crystallographic direction starts to contribute, seen to the right of [11-2-3], at an angle of about 30° . For an impact angle of 17° , figure 6(e), the probability is high for channeling along the [11-2-3] direction, as expected. The arrow in figure 6(e) points at the extremely high local concentration deep down along the [11-2-3], where the intensity scale has saturated. This means that very many of the ions are steered along the crystal channel [11-2-3] and stop at a similar depth. However, some ions may find their way to other direction and the probability for scattering into the [000-1] direction is not zero. In the performed simulations, no increased probability is found for scattering into channels parallel to the sample surface, perpendicular to the A-face. This kind of channeling have previously been predicted from simulations of Al implantations into 4H-SiC samples with 8° miscut angle but concentrations less than 10^{-4} of the maximum concentration is expected and may be too low in our simulations [41].

In addition, 3D simulations have also been made for a larger impact area of $1 \times 1 \mu\text{m}^2$, an area more relevant to present device dimensions. In figure 7 simulations for 200 keV $^{51}\text{V}^+$ ions impinging along the [000-1] direction are shown. The data is displayed as an 1D-image on a log-scale (a) and a 2D- top view (b), as well as a cross section on a linear scale (c). To display the 2D-image distribution in the $\{-1100\}$ plane a 10 nm thick slice has been cut out. In the top view all tracked ions are included as black dots and a yellow dashed line shows the size of the impact area, which is clearly smaller than the extension of the distribution at a certain depth.

A red line in the top view (figure 7(b)) shows where the data used in the cross section (figure 7(c)) has been taken. A pronounced contribution from channelled ions is revealed

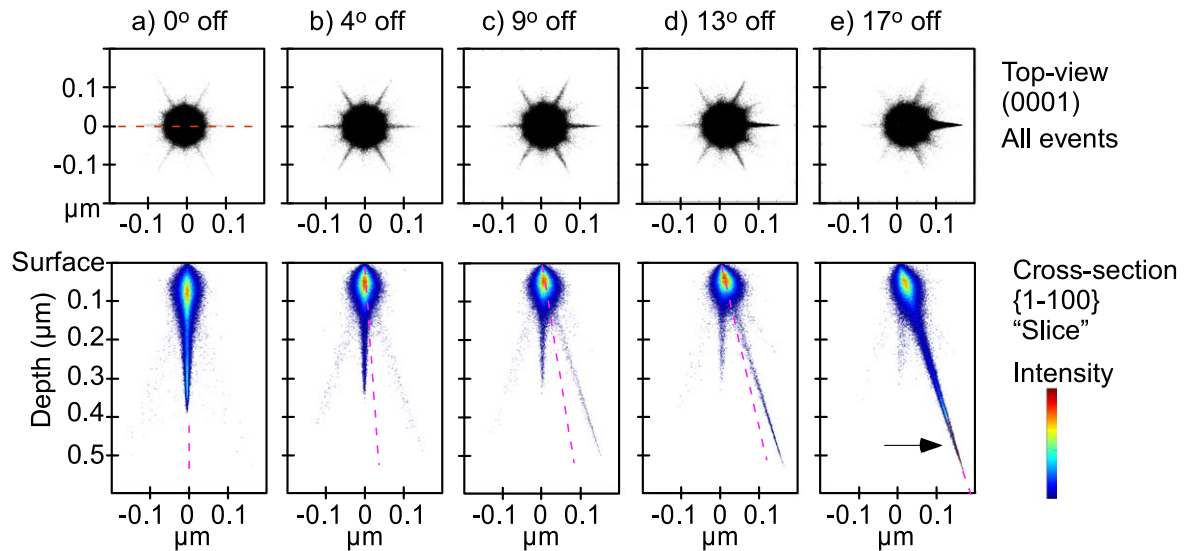


Figure 6. 3D-simulation of 100 keV $^{51}\text{V}^{+}$ -ions at impact angles of 0° (a), 4° (b), 9° (c), 13° (d) and 17° (e). In the simulation, an impact area of $1 \times 1 \text{ nm}^2$ has been used. On top, total amount of ^{51}V -ions from the whole volume is shown in black and below the cross section, represented by a slice in the $\{1-100\}$ plane, is displayed. The colours are used for the intensity scale. Dashed red lines indicate the implantation direction.

where the $[000-1]$ direction dominates. This finding is supported by simulations with a small impact area, $1 \times 1 \text{ nm}^2$, similar to figure 6(a), done for 100 keV (not shown for 200 keV). Using a larger impact area in the simulation results in overlap of parallel distributions and a broad band is seen between 0.25 and $0.6 \mu\text{m}$ in the 2D-image (figure 7(c)), where it is hard to distinguish between $[000-1]$ and $[11-2-3]$ directions. However, the total depth distribution correlates with a $[000-1]$ distribution (figure 6) and the shape of the distribution at the edge in the range of 0.25– $0.6 \mu\text{m}$ may give a hint about the relative contribution from the two channels. No expansion of the distribution by depth is present in this region, as expected for channeling along the $[000-1]$ direction. Closer to the surface, in the range 0– $0.25 \mu\text{m}$, at the edges of the implanted area, the distribution is laterally broader, $\sim 0.1 \mu\text{m}$, compared to the impact area and the concentration slowly decline with the lateral distance. This means that if an implantation is performed with a mask, some ions will be found underneath the mask and increase the lateral width of the distribution around the depth of the peak concentration.

4.4. Hot implantations

At elevated temperature, lattice vibration increases and an increasing number of ions may be dechanneled, resulting in a shallower profile. In addition to this enhanced dechanneling from thermal vibrations, a larger fraction of the ion induced damage will anneal due to dynamic annealing, leading to a lower degree of dechanneling. The influence of these two opposing effects of elevated temperatures is shown in figure 8, where experimental depth profiles for vanadium implantations at elevated temperatures are compared with results from the MC-BCA simulations. 200 keV ^{51}V ions were implanted into 4H-SiC along the $[000-1]$ direction (figure 8(a)) as well as at 4° off (figure 8(b)) with fluence in the range $(0.55\text{--}1.1) \times 10^{14} \text{ cm}^{-2}$. Both RT and elevated

temperatures have been used, starting with the RT implantation in the $[000-1]$ direction followed by implantation at 500°C and subsequent, implantations at 300°C and 150°C in different areas of the same sample. As the temperature increases, the box shaped profile for the $[000-1]$ implantation in figure 8(a) decreases slightly in depth but the main change is in the profile shape where concentration declines faster with depth due to an increasing dechanneling probability. In comparison with our previous results for Al implantations in 4H-SiC, the ^{51}V depth profile is less sensitive to an elevated temperature [11, 37].

If only the critical angles, based on atomic numbers of ion and target, are considered, a stronger temperature dependence would be expected for V. The different temperature sensitivity of the channeling effect between Al and V may be explained by larger available ‘channels’ for V-ions caused by the electronic structure of the impinging V-ion, leading to a stronger interaction with the target atoms. This effect is indicated by a decrease of the s parameter by a factor of two for V compared to Al.

For the 4° off implantation (figure 8(b)), the concentration and the penetration depth of channelled ions reduces between 0.35 and $0.7 \mu\text{m}$, as the temperature increases, although the depth profile is still broad and a small knee remains at a concentration of $2 \times 10^{16} \text{ cm}^{-3}$. The contribution from ions along the $[000-1]$ direction have declined but it is not absent even at 500°C .

Finally, it should be comment that to further improve the MC-BCA simulations a full cascade instead of the Kinching–Pease method has been used to describe ion implantation damage. For a full cascade, the number and position of displaced C and Si atoms during implantation is tracked and as a result an excellent agreement is obtained between experimental data and simulations as seen in figure 8(a) for the $[000-1]$ direction. Using the Kinching–Pease method, the ion

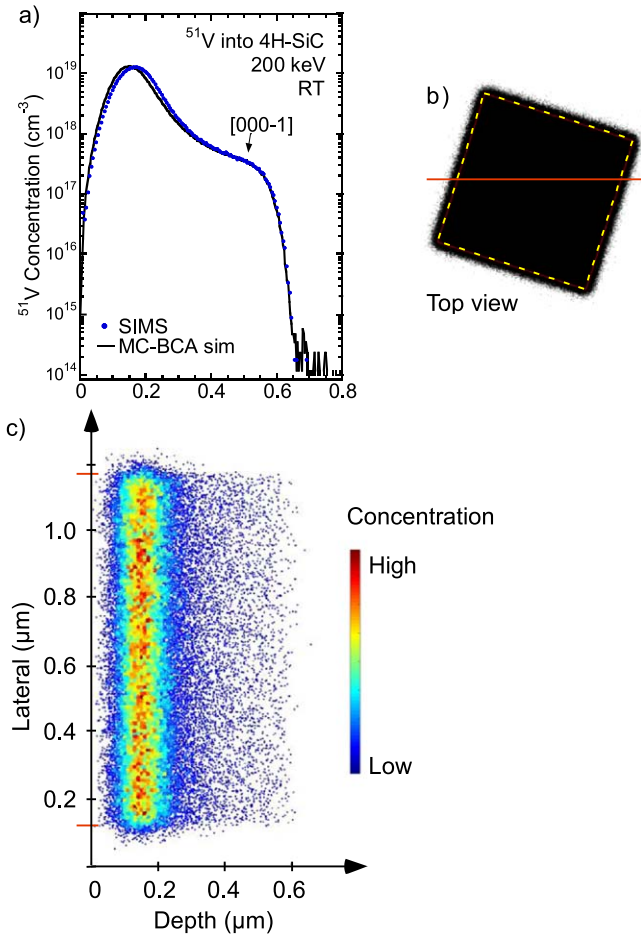


Figure 7. Comparison of SIMS measurements and 3D-simulated data for implantation of 200 keV ^{51}V in 4H-SiC. In (a) the simulated data is displayed as 1D- depth profile together with SIMS results. 2D-images show the depth and lateral distribution for (b) a cross section in a 10 nm thick slice in the $\{-1100\}$ plane and (c) a top-view in where the used position of the cross section is indicated by a red line and a yellow dashed line shows the impact area. All tracked ^{51}V -ions are included as black dots for the top-view, while the concentration is represented by a color scale in the cross section.

induced damage (created vacancies and interstitials) appears closer to the surface in the simulations and, as a result the main peak emerge closer to the surface as compared to experimental data and gives less accurate description of channeling along the $[000-1]$ direction (figures 5 and 7(a)). However, using a full cascade the simulation time is remarkable increased.

5. Summary

In this study, we present experimental results supported by MC-BCA simulations for intentional and unintentional ion channeling during implantations of $^{51}\text{V}^{+}$ -ions at energies between 50 and 300 keV in 4H-SiC at RT as well as at elevated temperatures. The incoming beam has been aligned in a 'random' direction, as well as along the crystal $[000-1]$ axis and at tilt angles from 0° , 4° , 9° , 13° and 17° in the $\{1-100\}$ plane have been investigated. For the random case, the

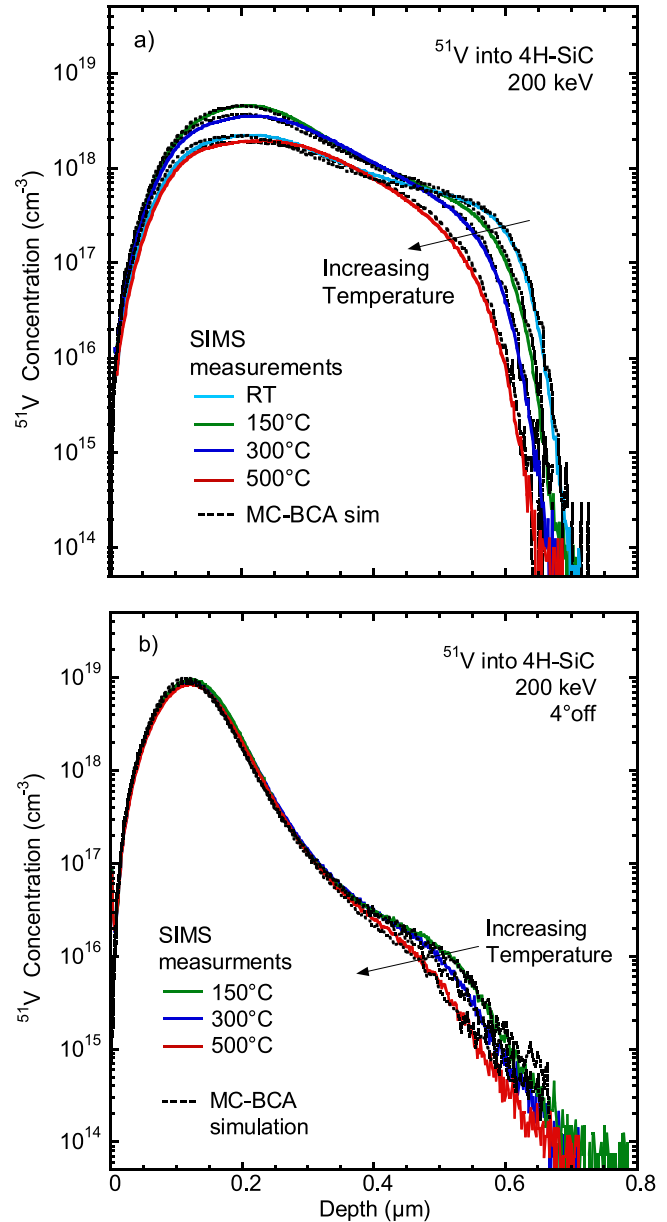


Figure 8. SIMS profiles showing the depth distribution of ^{51}V in 4H-SiC implanted in (a) the $[000-1]$ direction and (b) 4° off. The samples have been implanted with 200 keV $^{51}\text{V}^{+}$ -ions at RT, 150, 300 and 500 $^\circ\text{C}$ at fluence $(0.55-1.1)\times 10^{14}\text{ cm}^{-2}$. MC-BCA simulations of experimental data with SIIMPL have been added as black dotted lines.

electronic stopping, S_e , has been determined to $6E^{0.45}\text{ eV}/(\text{atoms cm}^{-2})$, which is used in simulations of V in 4H-SiC.

Experimental SIMS profiles, show a change between the dominant channeling direction from $[000-1]$ to $\langle 11-2-3 \rangle$ as the tilt angle is increasing from 0° to 17° . MC-BCA simulations indicate that independent of the used angle of incidence, some ions will always be scattered into the $[000-1]$ channel as well as the crystallographic members of the $\langle 11-2-3 \rangle$ family. These channelled ions interact less with the lattice and dissipate their energy over a longer distance than randomly incident ions. Hence, these channelled ions will always contribute to a deeper protrusion of the depth distribution and it will not be

possible to find a perfect non-channeling direction in 4H-SiC at RT, giving the distribution of ions implanted in an amorphous matrix. However, the channeling effect is slightly reduced at elevated temperatures due to increasing lattice vibration, although this effect is found to be limited in the energy and temperature range used here.


In addition to channeling, the vanadium ions will be laterally scattered and can for example be found outside the impact area under an implantation mask in device structures. No tendency of V to be scattered into the A-plane, parallel to the surface, is observed in the simulations.

Acknowledgments

Financial support by the Swedish Research Council (VR E0510501), the Ion Technology Centre, ITC, in Sweden via VR-RFI (contracts #821-2012-5144 & #2017-00646-9) and the Swedish Foundation for Strategic Research (SSF, contract RIF14-0053) and the Norwegian Research Council via the Norwegian Micro- and Nano-fabrication Facility (NORFAB 197 411/v30) are gratefully acknowledged.

ORCID iDs

M K Linnarsson  <https://orcid.org/0000-0002-0292-224X>

A Hallén  <https://orcid.org/0000-0002-8760-1137>

L Vines  <https://orcid.org/0000-0001-5759-7192>

References

- [1] Miyazawa T, Tawara T, Takanashi R and Tsuchida H 2016 *Appl. Phys. Express* **9** 11301
- [2] Hettler C, James C, Dickens J and Neuber A 2010 *IEEE International Power Modulator and High Voltage Conference* p 34
- [3] Mitchel W C, Mitchell W D, Landis G, Smith H E, Lee W and Zvanut M E 2007 *J. Appl. Phys.* **101** 013707
- [4] Nordlund K, Djurabekova F and Hobler G 2016 *Phys. Rev. B* **94** 214109
- [5] Nordlund K and Hobler G 2018 *Nucl. Instrum. Methods B* **435** 61
- [6] Vantomme A 2016 *Nucl. Instrum. Methods B* **371** 12
- [7] Gemmell D S 1974 *Rev. Mod. Phys.* **46** 129
- [8] Hobler G 1996 *Radiat. Eff. Defects Solids* **139** 21
- [9] Wong-Leung J, Janson M S and Svensson B G 2003 *J. Appl. Phys.* **93** 8914
- [10] Janson M S, Hallén A, Godignon P, Kuznetsov A Y, Linnarsson M K, Morvan E and Svensson B G 2000 *Mater. Sci. Forum* **338–342** 889
- [11] Linnarsson M K, Hallén A, Vines L and Svensson B G 2019 *Mater. Sci. Forum* **963** 382
- [12] Lazar M, Laariedh F, Cremillieu P, Planson D and Leclercq J L 2015 *Nucl. Instrum. Methods B* **365** 256
- [13] Suvorov A V and Pala V 2018 *US Patent* 2018/0069083 A1
- [14] Kimoto T, Kawahara K, Niwa H, Kaji N and Suda J 2014 *2014 Int. Workshop on Junction Technology (IWJT), IEEE Proc.* p 1
- [15] Hallén A and Linnarsson M K 2016 *Surf. Coat. Technol.* **306** 190
- [16] Michel A E, Kasti R H, Mader S R, Masters B J and Gardner J A 1984 *Appl. Phys. Lett.* **44** 404
- [17] Schreutelkamp R J, Saris F W, Westendorp J F M, Kaim R E, Odium G B and Janssen K T F 1989 *Mater. Sci. Eng. B* **2** 139
- [18] Morvan E, Mestres N, Campos F J, Pascual J, Hallén A, Linnarsson M and Kutznetsov A Y 2000 *Mater. Sci. Forum* **338–342** 893
- [19] Lorenz K, Wendler E, Redondo-Cubero A, Catarino N, Chauvat M-P, Schwaiger S, Scholz F, Alves E and Ruterana P 2017 *Acta Mater.* **123** 177
- [20] Lindhard J 1964 *Phys. Lett.* **12** 126
- [21] Lindhard J 1965 *Mat. Fys. Medd. Dan. Vid. Selsk.* **34** 14
- [22] Picraux S T, Davies J A, Eriksson L, Johansson N G E and Mayer J W 1969 *Phys. Rev.* **180** 873
- [23] Posselt M, Schmidt B, Feudel T and Strecker N 2000 *Mater. Sci. Eng. B* **71** 128
- [24] Lulli G, Albertazzi E, Bianconi M, Nipoti R, Cervera M, Carnera A and Celini C 1997 *J. Appl. Phys.* **82** 5958
- [25] Hobler G 1995 *Nucl. Instrum. Methods B* **96** 155
- [26] Morvan E, Godignon P, Montserrat J, Fernández J, Flores D, Millán J and Chante J P 1997 *Mater. Sci. Eng. B* **46** 218
- [27] Janson M 2003 *PhD Thesis* KTH- Royal Institute of Technology, Department of Microelectronics and Information Technology, Materials and Semiconductor Physics Laboratory, Sweden
- [28] Robinson M T and Oen O S 1963 *Phys. Rev.* **132** 2385
- [29] Robinson M T and Torrens I M 1974 *Phys. Rev. B* **9** 5008
- [30] Oen O S and Robinson M T 1976 *Nucl. Instrum. Methods* **132** 647
- [31] Barrett J H 1971 *Phys. Rev. B* **3** 1527
- [32] Ziegler J F, Biersack J P and Littmark U 1985 *The Stopping and Ranges of Ions in Solids* (Oxford: Pergamon)
- [33] Biersack J P and Haggmark L 1980 *Nucl. Instrum. Methods* **174** 257
- [34] Kinching G H and Pease R S 1955 *Rep. Prog. Phys.* **18** 1
- [35] Janson M S, Linnarsson M K, Hallén A and Svensson B G 2004 *J. Appl. Phys.* **96** 164
- [36] Zywiets A, Karch K and Bechstedt F 1996 *Phys. Rev. B* **54** 1791
- [37] Hallén A, Linnarsson M K and Vines L 2019 *Mater. Sci. Forum* **963** 375
- [38] Önnby C and Pantano C G 1997 *J. Vac. Sci. Technol. A* **15** 1597
- [39] Nuclear Energy Agency, data bank, computer service, SRIM-2008 (www.oecd-nea.org/tools/abstract/detail/nea-0919/)
- [40] Desalvo A, Galloni R, Rosa R and Zignani F 1980 *J. Appl. Phys.* **51** 1994
- [41] Lulli G 2011 *IEEE Trans. Electron Devices* **58** 190